Journal of Applied Fluid Mechanics, Vol. 9, No. 5, pp. 2581-2594, 2016.
Available online at www.jafmonline.net, ISSN 1735-3572, EISSN 1735-3645.
DOI: 10.18869/acadpub.jafm.68.236.25296

Simulation of Flow and Heat Transfer of Nanofluid in an Eccentric Annulus with Multicomponent Lattice Boltzmann Method

A. Rostamzadeh, E. Goshtasbi Rad and K. Jafarpur†

School of Mechanical Engineering, Shiraz University, Shiraz, Iran Molasadra Str., Shiraz, 71936-16548, Iran.

†*Corresponding Author Email: kjafarme@shirazu.ac.ir*

(Received July 13, 2015; accepted September 30, 2015)

ABSTRACT

In the present study, Lattice Boltzmann method is employed to investigate a two dimensional mixed convection heat transfer of Al_2O_3-water nanofluid in a horizontal annulus between a cold outer cylinder and the hot, rotating inner cylinder. To do so, the double lattice Boltzmann equation is utilized for the base fluid and the nanoparticles to describe the dynamic as well as the thermal behavior of nanofluid. Moreover, different forces such as Brownian, drag and gravity acting on the nanoparticles are taken into consideration. Calculations have been performed for Rayleigh number ranging from 10^3 to 2×10^4, Reynolds number from 5 to 120, vertical and horizontal eccentricity from -0.75 to 0.75 with volume fraction of nanoparticles from 0 to 0.1. The current computational results reveal that by adding nanoparticles, the mean Nusselt number for Ra $<10^4$ increases as Rayleigh number increases while in the case of Ra $>10^4$, it decreases. Also, with Re>80, the mean Nusselt number increases with increasing Reynolds number; although for low Reynolds number this rising trend is not observed. Besides, when the inner cylinder moves vertically upward from the center, the addition of nanoparticles increases Nusselt number relative to the base fluid.

Keywords: Nanofluid; Multicomponent lattice Boltzmann method; Heat transfer; Eccentric annulus; Nanoparticles.

NOMENCLATURE

e	lattice speed	α	thermal diffusivity
e_i	discrete particle speed	φ	volume fraction
F	external forces	β	thermal expansion coefficient
FB	buoyancy force	υ	kinematic viscosity
f	density distribution function	μ	dynamic viscosity
f^{eq}	equilibrium density distribution function	ρ	fluid density
g	energy distribution function	τ	relaxation time
g^{eq}	equilibrium energy distribution function	θ	dimensionless temperature
Nu	Nusselt number	σ	components (σ=1, 2, water and nanoparticles)
Pr	Prandtl number	**subscript**	
Ra	Rayleigh number	nf	nanofluid
Re	Reynolds number	f	base fluid
k	thermal conductivity	p	solid particle
g_y	gravitational force	eq	equilibrium distribution function
k_B	Boltzmann constant	neq	non-Equilibrium distribution function
c	the lattice constant divided by the time step	i	lattice velocity direction

1. INTRODUCTION

Mixed convection in the concentric and eccentric horizontal annuli is widely employed in a variety of heat transfer systems such as food processing (Prudhomme *et al*. 1993),electrical component systems (Abedini *et al*., solar collector processing, double heat exchangers (Fattahi *et al*. 2011) and

journal bearing. Recently with the development of technology, the demand for energy has increased worldwide. Hence, the researchers constantly look for new methods to increase the thermal performance of different systems. Using liquid dispersion of solid nanoparticles (nanofluids) is a recent method that enhances thermal performance relative to traditional fluids such as water, oil or ethylene glycol. This novel technique was first introduced by Choi (1995) in order to develop advanced heat transfer fluids. Afterwards, many researchers investigated the effects of nanofluids on the forced convection heat transfer. They proved that the nanoparticles suspensions are more likely to enhance the heat transfer (Trisaksri and Wongwises 2007,Wang and Mujumdar 2007, Wen *et al*. 2009, Saidur *et al*. (2011), Fan and Wang (2011), Sarkar (2011)). On the other hand, relatively few works have been performed on natural or mixed convection heat transfer in nanofluids especially in annulus. As regards the convective flow of nanofluids in annulus, Abu-Nada *et al*. (2008) numerically studied the natural convection of nanofluids in a concentric annulus. They presented the effect of nanoparticles on heat transfer in the various ranges of Rayleigh number and nanoparticles volume fraction. Cianfrini *et al*. (2011) theoretically conducted the natural convection heat transfer of nanofluid flow in horizontal concentric cylinders maintained at different uniform temperatures. The results revealed that increasing nanoparticle volume fraction, increases the heat transfer coefficient and the highest heat transfer rate relates to the smallest nanoparticles size. Natural convection of copper-water nanofluid in a vertical annulus channel was numerically investigated by Shahi *et al*. (2011). They showed that the Nusselt number increases as nanofluids concentration increases. Habibi and Pop (2013) conducted a numerical study of the natural heat transfer to Cu-water nanofluid flow in a horizontal eccentric cylinder. They examined the effect of eccentricity and volume fraction of nanoparticles on the Nusselt number. Their results are in good agreement with previous investigations. Ashorynejad *et al*. (2012) and Parvin *et al*. (2012) investigated the natural convection of nanofluids in a concentric annulus by considering the magnetic field effects and the thermal conductivity variations. Also, the transient natural convection heat transfer of aqueous nanofluids in a horizontal concentric annulus has been studied by Yu *et al*. (2012).

In general, the mixture of nanoparticles and base fluid could be approximated as a single component or modelled as a multicomponent medium. The mentioned works have investigated the convective heat transfer in the horizontal annulus based on the homogeneous or single-phase approach. It is obvious that under the effect of forces and potentials that exerted on the nanofluids, the results obtained for multicomponent model will be more precise compared to those of one component model.

As an effective numerical approach, it was shown that the Lattice Boltzmann method (LBM) has the ability to incorporate the complex physics of multi phase and multi component flows. LMB considers the external and internal forces on the nanoparticles. Also, mechanical and thermal interactions between the nanoparticles and fluid molecules can be modelled by LBM. Xuan and Yao (2005) have developed multicomponent Lattice Boltzmann method to simulate flow and energy transport occurring inside nanofluids. Afterwards, a novel hybrid method of multicomponent and single component was proposed by Zhou *et al*. (2010) to examine flow and thermal processes of the nanofluid. In addition, with regard to the investigation of thermal transport in nanofluid, Zarghami *et al.* (2013) have developed a cell-centered finite-volume formulation for a multicomponent thermal Lattice Boltzmann method. Based on these studies, the multi component LBM is an acceptable method to simulate the nanofluids as a two components media.

According to the literature, the effect of nanofluid in mixed convection heat transfer inside the eccentric annulus with inner rotating cylinders, which is a complex geometry has not been examined yet. In this paper, a mixed convection flow and heat transfer in a horizontal two–dimensional annular space between two eccentric cylinders filled with Al_2O_3–Water nanofluid are studied numerically. The results are obtained for different ranges of Rayleigh and Reynolds numbers and eccentricity. In addition, with Multi component LBM it is possible to obtain the distribution of nanoparticles, which is very important in practical applications.

2. MODEL DESCRIPTION

2.1 Multicomponent Lattice Boltzmann Method

In order to simulate the fluid domain containing nanoparticles and base fluid, a description of the multicomponent LBM developed by Xuan and Yao (2005) is presented. Two-particle distribution function is needed to simulate nanofluids in this method, the density distribution function for hydrodynamics and the temperature distribution function for the thermal field.

2.1.1 Density Distribution Function

The LBM is a mesoscopic approach with fictive particles that consecutively propagate and collide over a discrete mesh. The particle distribution function $f_i^{\sigma}(x,t)$ is the amount of particle at node x, time t, and velocity e_i. The superscript "σ" labels the fluid component and the subscript "i" indicates the velocity direction. The particle distribution function satisfies the lattice Boltzmann equation. Generally, in multicomponent media such as nanofluids, there are internal and external forces between different components. Therefore, the LBM should be modified accordingly. Based on the study carried out by Buick and Greated (2000), by taking forces into consideration, Lattice Boltzmann equation can be written as:

$$f_i^{\sigma}\left(x+e_i\Delta t,t+\Delta t\right)-f_i^{\sigma}\left(x,t\right)= -\frac{1}{\tau^{\sigma}}\left(f_i^{\sigma}\left(x,t\right)-f_i^{\sigma,eq}\left(x,t\right)\right) + \frac{2\tau^{\sigma}-1}{2\tau^{\sigma}}\frac{D\Delta t}{B_i c^2}F^{\sigma}.e_i \quad for\ \sigma=1,2 \tag{1}$$

Where the first expression in the right-hand side is the collision operator, which represents the change rate of the particle distribution due to collisions and $f_i^{\sigma,eq}\left(x,t\right)$ is the equilibrium distribution at x, t. τ^{σ} is the relaxation time that controls the rate of approach to equilibrium. F^{σ} is the vector sum of all forces acting on the σth component of the nanofluid per unit lattice volume, D is the dimension; B_i is the adjustable coefficient. The equilibrium distribution function can be represented in the following form for particles of each type (He and Luo 1997) :

$$f_i^{\sigma,eq}=\omega_i\rho^{\sigma}\left(1+3\frac{\left(e_i.u^{\sigma,eq}\right)}{c^2}+\frac{9}{2}\frac{\left(e_i.u^{\sigma,eq}\right)^2}{c^4}-\frac{3}{2}\frac{\left(e_i.u^{\sigma,eq}\right)^2}{c^2}\right)$$

$$\omega_i=\begin{cases}4/9 & i=0\\ 1/9 & i=1,...,4\\ 1/36 & i=5,...,8\end{cases} \tag{2}$$

Where ω_i denotes the weight coefficient. Macroscopic quantities such as density $\rho^{\sigma}\left(x,t\right)$ and the fluid velocity u^{σ}particle distribution function may be written as follows (Xuan and Yao 2005):

$$\rho^{\sigma}\left(x,t\right)=\sum_i m^{\sigma}f_i^{\sigma}\left(x,t\right)$$

$$u^{\sigma}\left(x,t\right)=\frac{\sum_i m^{\sigma}f_i^{\sigma}\left(x,t\right)e_i}{\rho^{\sigma}\left(x,t\right)} \tag{3}$$

Where m^{σ} represents the molecular mass of the σth component. The equilibrium velocity is $u^{eq}=\sum_{\sigma}\frac{\rho^{\sigma}u^{\sigma}}{\tau^{\sigma}}\Big/\sum_{\sigma}\frac{\rho^{\sigma}}{\tau^{\sigma}}$ and the equilibrium velocity of each component in the presence of forces is (Buick and Greated 2000):

$$u^{\sigma,eq}=u^{eq}+\frac{F^{\sigma}\Delta t}{2\rho^{\sigma}} \tag{4}$$

The kinematic viscosity of each component and the mean kinematic viscosity of the nanofluid are calculated as follows: $\nu^{\sigma}=\frac{2\tau^{\sigma}-1}{6}c^2\Delta t$ and $\nu=\frac{2\sum_{\sigma}\overline{\rho^{\sigma}}\tau^{\sigma}-1}{6}c^2\Delta t$ where $\overline{\rho^{\sigma}}=\rho^{\sigma}\Big/\sum_{\sigma}\rho$ is the concentration of each component.

In order to incorporate the buoyancy force term (caused by temperature gradient) in the model, an extra term $(\Delta t\, e_i.FB_i^{\sigma})$ should be added to the right hand side of the momentum Eq. (1) and needs to be calculated from Eq. (5) (Mohamad 2011):

$$\Delta t\, e.FB^{\sigma}=3\rho^{\sigma}\omega(i)g_x\beta^{\sigma}(T^{\sigma}-T_{ref})\ e_x + 3\rho^{\sigma}\omega(i)g_y\beta^{\sigma}(T^{\sigma}-T_{ref})\ e_y \tag{5}$$

2.1.2 Temperature Distribution Function

For the thermal LBM, the same approach as the one for hydrodynamic method is developed. The evolution equation of the temperature distribution function is (Xuan and Yao 2005):

$$g_i^{\sigma}\left(x+e_i\Delta t,t+\Delta t\right)-g_i^{\sigma}\left(x,t\right)= -\frac{1}{\tau_{\theta}^{\sigma}}\left(g_i^{\sigma}\left(x,t\right)-g_i^{\sigma,eq}\left(x,t\right)\right) \tag{6}$$

Where τ_{θ}^{σ} is the relaxation time for the thermal model. In addition, the energy equilibrium distribution function is calculated as follows:

$$g_i^{\sigma,eq}=\omega_i\theta^{\sigma}\left(1+3\frac{\left(e_i.u^{eq}\right)}{c^2}+\frac{9}{2}\frac{\left(e_i.u^{eq}\right)^2}{c^4}-\frac{3}{2}\frac{\left(e_i.u^{eq}\right)^2}{c^2}\right)$$

$$\theta^{\sigma}\left(x,t\right)=\sum_i g_i^{\sigma}\left(x,t\right) \tag{7}$$

Where $\theta^{\sigma}\left(x,t\right)$is the internal energy variable of the σth component. The mean temperature of the nanofluid at every lattice point and thermal diffusivity of the nanofluid can be respectively written as (Inamuro *et al*. 1995):

$$T\left(x,t\right)=\frac{\sum_{\sigma}\sum_i g_i^{\sigma}}{\sum_{\sigma}\rho^{\sigma}c_p^{\sigma}} \tag{8}$$

$$\alpha=\frac{2\sum_{\sigma}\overline{\rho^{\sigma}}\tau_{\theta}^{\sigma}-1}{6}c^2\Delta t \tag{9}$$

2.2. Boundary Conditions

The new modified models of curve boundary condition for LBM are proposed by (Huang *et al*. 2006, Yan and Zu 2008). They showed that LBM have acceptable results with regard to temperature and velocity curve boundary conditions. In the current study, the curved non slip wall boundary condition proposed by Yan and Zu (2008) is used for velocity field. The fraction of an intersected link in the fluid region, Δ, as shown in Fig. 1 , is defined as $\Delta=\left|x_f-x_w\right|/\left|x_f-x_b\right|$ where x_f and x_b represent the boundary nodes in fluid and solid region respectively. Also, x_w denotes intersections of the boundary with various lattice links. The Chapmann-Enskog expansion for the post collision distribution function is given by the following equation:

$$\tilde{f}_i^{\sigma}(x_b,t)=\tilde{f}_i^{\sigma}(x_f,t)-\chi\left[\tilde{f}_i^{\sigma}(x_f,t)-\tilde{f}_i^{\sigma,eq}(x_f,t)\right]+$$

$$\omega_i \rho^{\sigma}(x_f,t)\frac{3}{c^2}e_i.[\chi(u_{bf}-u_f)-2u_w] \tag{10}$$

Where

$$u_{bf}=u_{ff}=u(x_{ff},t),\ \chi=\frac{(2\Delta-1)}{(\tau-2)},\ if\ 0\le\Delta\le\frac{1}{2}$$
$$u_{bf}=\frac{1}{2\Delta}(2\Delta-3)u_f+\frac{3}{2\Delta}u_w,\ \chi=\frac{(2\Delta-1)}{(\tau-1/2)},\ if\ \frac{1}{2}\le\Delta\le1 \tag{11}$$

In the Eq. (11), $e_i^{\sim}=-e_i$; $x_{ff}=x_f+e_i^{\sim}\delta t$; u_f is the fluid velocity near the wall; u_w denotes the velocity of the solid wall and u_{bf} is an imaginary velocity for intersections.

The thermal curved boundary condition for specifying the post-collision distribution function, based on (Huang *et al*. 2006), is obtained from:

$$\tilde{g}_i^{\sigma}(x_w,t)=g_i{}^{\sigma,eq}(x_w,t)+(1-\frac{1}{\tau_\theta^{\sigma}})g_i{}^{\sigma,neq} \tag{12}$$

Where g_i^{neq} is the nonequilibrium part of temperature distribution function. The first term of right hand side is determined by Eq. (7) with the following parameters

$$\rho_w=\rho(x_w+e_i)=\rho_f$$
$$\theta_w=\begin{cases}\Delta T_{w1}+(1-\Delta)T_{w2} & if\ \ \Delta\ge0.75\\ T_{w1} & if\ \ \Delta\prec0.75\end{cases} \tag{13}$$
$$\begin{cases}T_{w1}=(\theta_b+(\Delta-1)\theta_f)/\Delta\\ T_{w2}=(2\theta_b+(\Delta-1)\theta_{ff})/(1+\Delta)\end{cases}$$

And the second term in Eq. (12) is:

$$g_i{}^{neq}(x_w,t)=\Delta g_i{}^{neq}(x_f,t)+(1-\Delta)g_i{}^{neq}(x_{ff},t)$$
$$g_i{}^{neq}(x_f,t)=g_i\ (x_f,t)-g_i{}^{eq}(x_f,t) \tag{14}$$

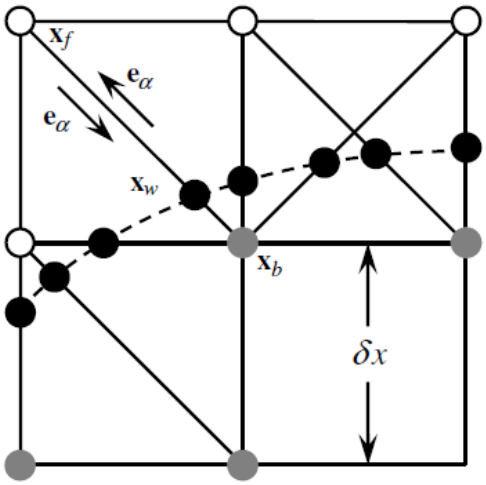

Fig. 1. Layout of the regularly spaced lattices and curved wall boundary.

2.3 Dynamic Forces on Nanofluids

To describe the dynamic of nanofluids as a colloidal suspension, all forces or potentials influencing numerical system such as Brownian, gravitational, drag, buoyancy forces, in addition to the interaction potentials should be taken into consideration.

The gravitational force in nanofluid is calculated as follows:

$$F_H=-\frac{4}{3}\pi a^3 g_y\Delta\rho \tag{15}$$

Where "a" denotes the radius of nanoparticles, $\Delta\rho$ is the difference of mass density between nanoparticle and the base liquid.

The drag force can be expressed as:

$$F_D=-6\pi\mu a\Delta u \tag{16}$$

Where μ is the viscosity of the fluid, Δu signifies the velocity difference between the particle and the liquid.

Brownian force in random direction is calculated using Eq. (17) (He and Ahmadi 1999):

$$F_B(t)=G_i\sqrt{\frac{C}{dt}}\qquad C=12\pi\mu a k_B T \tag{17}$$

Where G_i is a Gaussian random number with zero mean and unit variance, k_B is the Boltzmann constant, dt is a time step and T is the absolute temperature of the fluid.

The potential interaction between the nearest neighbor nanoparticles is given by (Russel *et al*. 1992):

$$V_A=-\frac{1}{6}A\left(\frac{2a^2}{r^2-4a^2}+\frac{2a^2}{r^2}+\ln\frac{r^2-4a^2}{r^2}\right) \tag{18}$$

Where A is Hamaker constant and r is distance between nanoparticles.

For all nanoparticles within the adjacent lattices in the D2Q9 model, the force caused by the interaction potential is written as:

$$F_A=\sum n_i\frac{\partial V_A}{\partial r_i} \tag{19}$$

Where n_i is the number of the particles within the adjacent lattice i, $n_i=\rho_p V/m_p$ (V represents the volume of single grid and m is the mass of a single nanoparticle).

3. MATHEMATICAL MODEL

In this article, heat transfer characteristic of Al_2O_3-water nanofluid within a two dimensional horizontal eccentric annuli with rotating inner cylinder is studied. The inner cylinder is maintained at a constant temperature T_1 and the temperature of outer cylinder is set at a constant temperature T_2. It

is presumed that $T_1 > T_2$, the same assumption which has been made in the previous researches. Numerical results are obtained for the volume fraction of nanoparticles ranging from 0 to 0.1, the Reynolds number from 5 to 120, the eccentricity from -0.75 to 0.75 and the Rayleigh number from10^3 to 2×10^4. The ratio of outer cylinder radius to inner cylinder (η) is considered as 2.6. The geometry of the annulus is illustrated in Fig. 2.

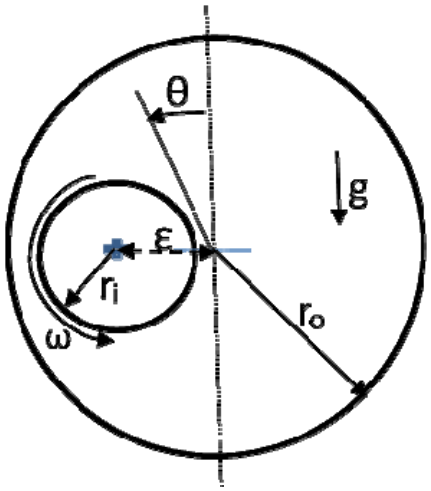

Fig. 2. Schematic diagram of the problem.

The Reynolds and Rayleigh numbers for the current problem and the geometric parameter of eccentricity (e) are defined as follows:

$$\mathrm{Re} = \omega_i\, r_i \left(r_o - r_i\right)/\upsilon,$$

$$Ra = g\beta\Delta T \left(r_o - r_i\right)^3/\alpha\upsilon, \qquad e = \frac{\varepsilon}{r_o - r_i} \tag{20}$$

ε is the distance between axes of inner and outer cylinders of eccentric annulus. The local Nusselt number on inner and outer cylinder are defined as:

$$Nu_i = r_i \frac{k_{nf}}{k_f \left(T_i - T_o\right)} \frac{\partial T}{\partial r}\bigg|_{r=r_i}$$

$$Nu_o = r_o \frac{k_{nf}}{k_f \left(T_i - T_o\right)} \frac{\partial T}{\partial r}\bigg|_{r=r_o} \tag{21}$$

Then, the mean Nusselt number is determined from:

$$\overline{Nu_i} = \frac{1}{2\pi}\int_o^{2\pi} Nu_i\left(\theta\right) d\theta$$

$$\overline{Nu_o} = \frac{1}{2\pi}\int_o^{2\pi} Nu_o\left(\theta\right) d\theta \tag{22}$$

$$\overline{Nu} = \left(\overline{Nu_i} + \overline{Nu_o}\right)/2$$

The computational convergence criterion is given as:

$$\max_{Grid}\left|\Gamma^{n+1} - \Gamma^n\right| < 10^{-7} \tag{23}$$

Where Γ denotes the independent variables (u, v, T) and *n* is the iteration number. It was shown that 60000 iterations were enough for the steady state condition for all the investigated values.

To attain the grid independency, the mean Nusselt number in the concentric rotational annulus with Pr=0.7, Ra=10^3, Re=20 and η= 2.6 are tested for different mesh sizes. The results are listed in Table 1.

Table 1 The mean Nusselt number for different grid sizes

Mesh size	80×80	100×100	150×150	200×200
$\overline{Nu}$	1.5015	1.5122	1.5135	1.5132

It is found that the variation of mean Nusselt number among all mesh sizes is not significant. Hence, a 100×100 grid size for the computational domain is employed.

In order to validate the computational code, isotherm and streamline patterns have been compared under pure natural convection, with the experimental data obtained by Guj and Stella (1995) and also the numerical result of (Abu-Sitta *et al*. 2007) as shown in Fig. 3.

Also in Fig. 4, the mean Nusselt number of mixed convection with Ra=10^3, Pr=0.7, Re=20 under different values of horizontal eccentricities are compared with the previous numerical work of (Abedini *et al*. 2014). The comparisons as depicted in Figs. 3 and 4 display good agreement between the current results and the available data (Guj and Stella 1995, Abu-Sitta *et al*. 2007, Abedini *et al*. 2014).

In the present work, the base fluid was water and Al_2O_3 nanoparticles were added to base fluid. The thermo-physical properties of the selected nanoparticles and water at $20^\circ C$ are given in Table 2.

On the other hand, to validate multicomponent LBM, the Nusselt number distribution around the inner cylinder surface for Al_2O_3-water nanofluid is computed and together with the results of Abu-Nada *et al*. (Abu-Nada *et al*. 2008) are displayed in Fig. 5. Rayleigh number, volume fraction of nanoparticles, and $(r_o\text{-}r_i)/2r_i$ ratio are $Ra = 10^3$, $\varphi = 0.1$ and 0.8, respectively. It is found that the results of present multicomponent LBM code is not only acceptable but also, accurate.

3. RESULTS AND DISCUSSION

4.1 Effect of Reynolds Number on Fluid Flow and Heat Transfer in the Annulus

As pointed out above, the main objective of the current study is to examine the characteristic of the mixed convection heat transfer in an annulus with nanofluids. Thus, the effect of Reynolds number on fluid flow and heat transfer of Al_2O_3-water

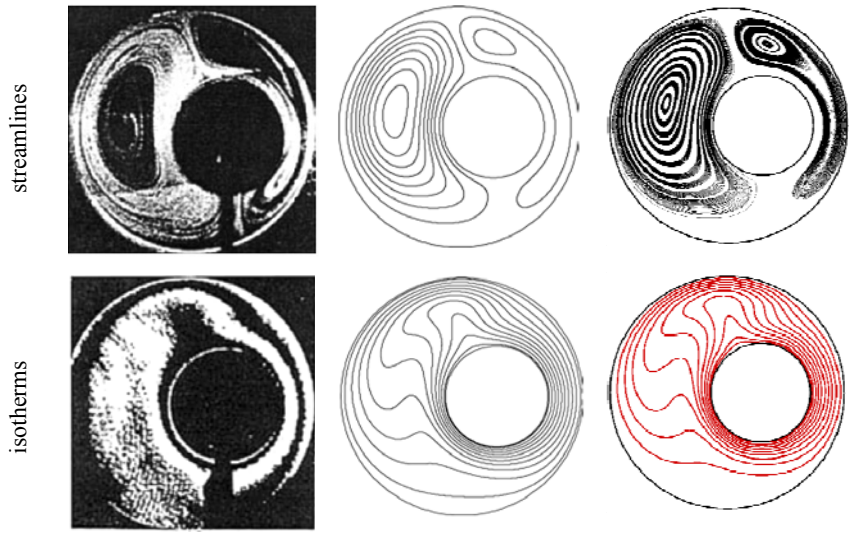

Fig. 3. Comparison of results; $Ra = 5.3\times10^3$, $\Pr = 0.71$, $e = 0.5$, $\dfrac{2r_i}{r_o - r_i} = 1.47$ **.**

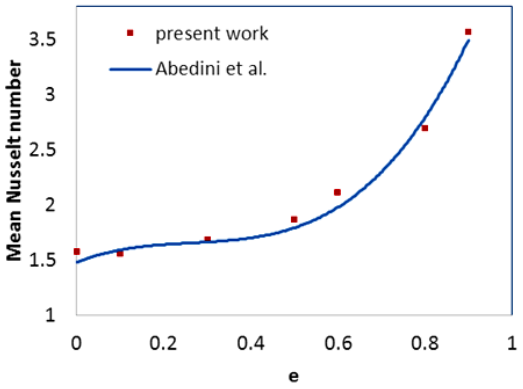

Fig. 4. Comparison of mean Nusselt number versus various eccentricities with previous numerical work (Abedini *et al.* 2014), at Ra=10^3, Pr=0.7 and Re=20.

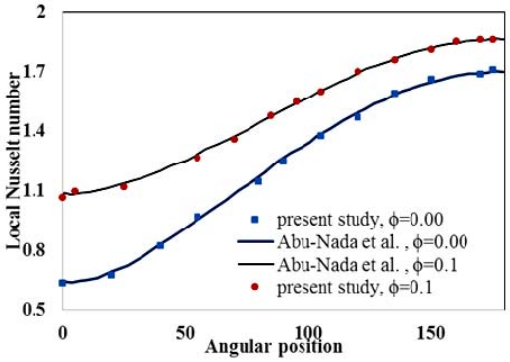

Fig. 5. Comparison of local Nusselt number from the present study with that of Abu-Nada *et al.* (2008) results. (Ra=10^3, Pr = 6.2, (r_o-r_i)/2r_i = 0.8).

Table 2. Thermo-physical properties of water and nanoparticle

	$\rho(kg/m^3)$	$C_p(J/kg\,K)$	k(W/m K)	$\alpha\times10^7(m^2/s)$
Water (Bejan 2013)	997.1	4179	0.613	1.47
Al_2O_3 (Abu-Nada 2009)	3890	775	31.8	105

nanofluid in the eccentric annulus is investigated, as well. Fig. 6 shows the patterns of streamlines and the isotherms in an eccentric annulus with fixed Ra=10^4, e= (0.5, +π/2) and 0.05 volume fraction of nanoparticles while the Reynolds number is varied between 5 and 120. According to Fig. 6, for all Reynolds numbers, the isotherms and the streamlines become more uniform by adding nanoparticles. By further increasing the Reynolds number, the isotherms are whirled in the rotational direction of the inner cylinder and the number of rings of streamlines around the inner cylinder will increase. Moreover, the increase in Reynolds number causes the isotherm spacing in the vicinity of the inner cylinder to increase and a corresponding reduction in a temperature gradient and the mean Nusselt number. Also, the weak vortex in left region gradually disappeared. Similar effects are observed when nanofluids are used.

The mean Nusselt number for different volume fractions of nanoparticle and Reynolds number is presented in Fig. 7. As shown in this figure, the increase in Reynolds number, which causes the reduction in buoyancy forces, will result in a decrease in Nusselt number for both base fluid and nanofluid. In other words, with increasing

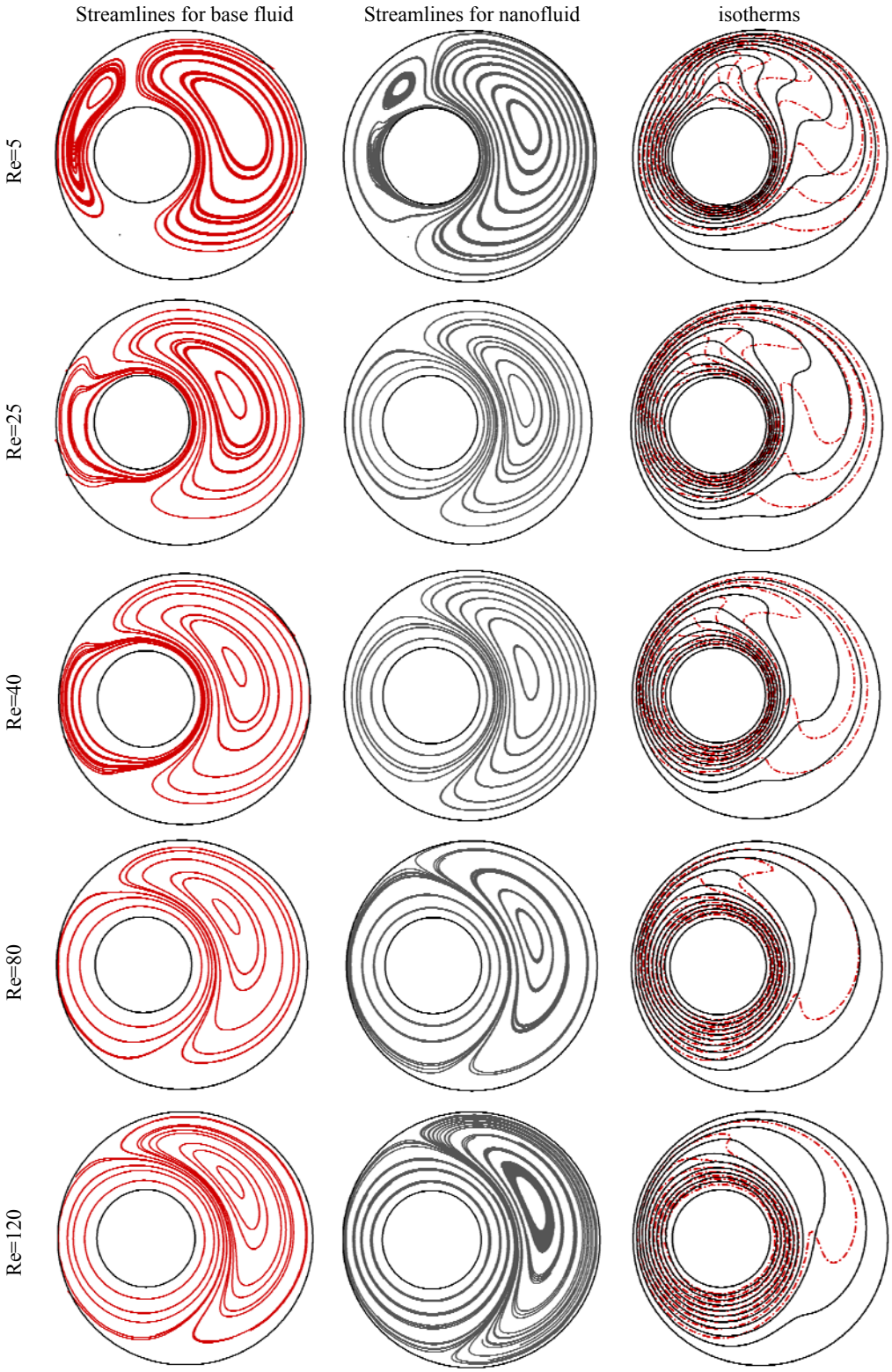

Fig. 6. Streamlines and isotherms patterns for nanofluid (solid line) and base fluid (dash line) at various Reynolds number, Ra=10^4, e= (1/2, π/2).

Reynolds number, the isotherms slowly assume a circular shape with the cylinders and ultimately the energy transport is dominated by the conduction heat transfer. Accordingly, for high Reynolds number (Re>40), there is a further increase with volume fraction of nanoparticles of the mean Nusselt number, as can be seen from Fig. 7 (by enhancement of effective thermal conductivity). However, for Re<40, the same trend is not observed; as φ_p is increased in the ranges of 0-0.01 and 0.05-0.1, the Nusselt number increases while in the other ranges it decreases.

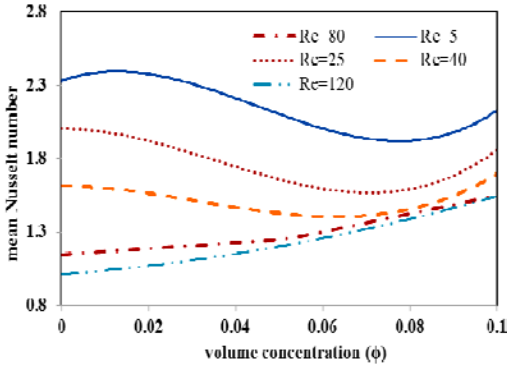

Fig. 7. Variation of mean Nusselt number with volume fraction of nanoparticles for various Reynolds number.

4.2 Effect of Rayleigh Number on Flow Pattern and Temperature Distribution

Figure 8 depicts the effect of Rayleigh number on streamlines and isotherms for the nanofluid with $\varphi = 0.05$ and the base fluid. These investigations are conducted at fixed Re equal to 25 and e = (-1/2, π/2). By increasing the Rayleigh number, obviously, the buoyancy forces will increase. Hence, concentric streamlines that are induced due to rotation of inner cylinder are gradually distorted at initial direction and in Ra=20000 one vortex in the left section of annulus is generated. Also, the increasing buoyancy force leads to the stronger convection effects and the augmentation of the thermal plume.

The mean Nusselt number versus Rayleigh number for various volume concentration of nanoparticles is reported in Fig. 9. It is observed that, the isotherms come closer to the inner cylinder as Ra increases, indicating large temperature gradient, using nanofluid lessens the strength of vortices and consequently decreases the temperature gradient and the Nusselt number except for φ = 0.01. On the other hand, the present results of Figs. 8 and 9 reveal that at low Ra $(Ra \le 4000)$ the mean Nusselt number increases with an increase in volume fraction of nanoparticles. For this range of Ra, no significant change is observed in the temperature gradient of nanofluid and base fluid. Therefore, enhancement of the effective thermal conductivity (by adding the nanoparticles) will augment the Nusselt number.

4.3. Effect of Eccentricity (Horizontal and Vertical Directions) on Fluid Flow and Heat Transfer

The effect of eccentricity in both horizontal and vertical directions at various locations is examined. In Fig. 10, the effect of the horizontal eccentricity on the flow pattern and isotherms for the base fluid and the nanofluid with Re=25 and Ra $=10^4$ are presented. The results indicate that, when the inner cylinder is moved horizontally in the right direction, two vortices can be seen in the annulus. These vortices, which cause high velocity gradient, change the isotherms and increase the heat transfer. In this situation, adding nanoparticles reduces the strength of vortices and the thermal plume as well. Also, when the inner cylinder is moved closer to the outer cylinder for both the base fluid and the nanofluid, the thermal plume intensifies. The effect of eccentricity on the mean Nusselt number is shown in Fig. 11. It is observed from Fig. 11(a) (horizontal eccentricity) that the Nusselt number is higher when the eccentricity is e= (+3/4, -π/2). Moreover, by using nanofluids, the temperature gradient and the effect of convection heat transfer decreases. In the same way, Nusselt number increases by increasing volume concentration of nanoparticles, if augmentation of the thermal conductivity of nanofluid becomes larger than the reduction in temperature gradient, for example e= (+3/4, π/2) (see Fig. 11).

Fig. 11(b) displays the effect of the vertical eccentricity on Nusselt number. When the inner cylinder is placed at larger distance from the center, the intensity of convection heat transfer decreases since the narrow space above the inner cylinder prevents the circulation of the hot fluid. As a result, the heat transfer by conduction is greater than the convection one. Therefore, as illustrated in Fig. 11(b), by adding nanoparticles, heat transfer and Nusselt number increase relative to the base fluid. Also, an increase in volume concentration of nanoparticles amplifies this enhancement. However, when the inner cylinder moved downward while the convection heat transfer was dominant, the inverse phenomena occurred: the Nusselt number decreased by adding nanoparticles.

4.4 Nanoparticles Distribution

There are interaction forces between base fluid and nanoparticles that affect the behavior of the nanofluid. These forces in the absence of centrifugal force are compared to buoyancy force caused by the temperature gradient. The buoyancy force is at least 10^6 times larger than the other interaction forces. Therefore, the interaction forces do not have a significant influence on the flow field. However, Brownian force is greater than the drag, interaction potential and gravity forces. This force affects the nanoparticle volume fraction distribution and leads to non-uniform contour lines (see Figs. 12 and 13).

Fig. 12 shows the distribution of nanoparticle volume concentration at fixed Re=25, φ=0.05 and various Rayleigh numbers. As illustrated in this figure, in low centrifugal force (Re=25), the buoyancy force plays an effective rule on mixed convection. This distribution is non-uniform for all Rayleigh numbers. Moreover, when buoyancy force increases, the distribution of nanoparticle volume concentration is more non-uniform and is enhanced in the direction of buoyancy force.

The effect of Reynolds number on the nanoparticle volume fraction is shown in Fig. 13. It is observed that by increasing Reynolds number (increasing the rotation of the inner cylinder), new contours are formed from the interaction of centrifugal and buoyancy forces (compare Figs. 13(a) with 13(d)). As it was described before, some of the nanoparticles are driven to the top of annulus due to buoyancy force, while some others are driven out to

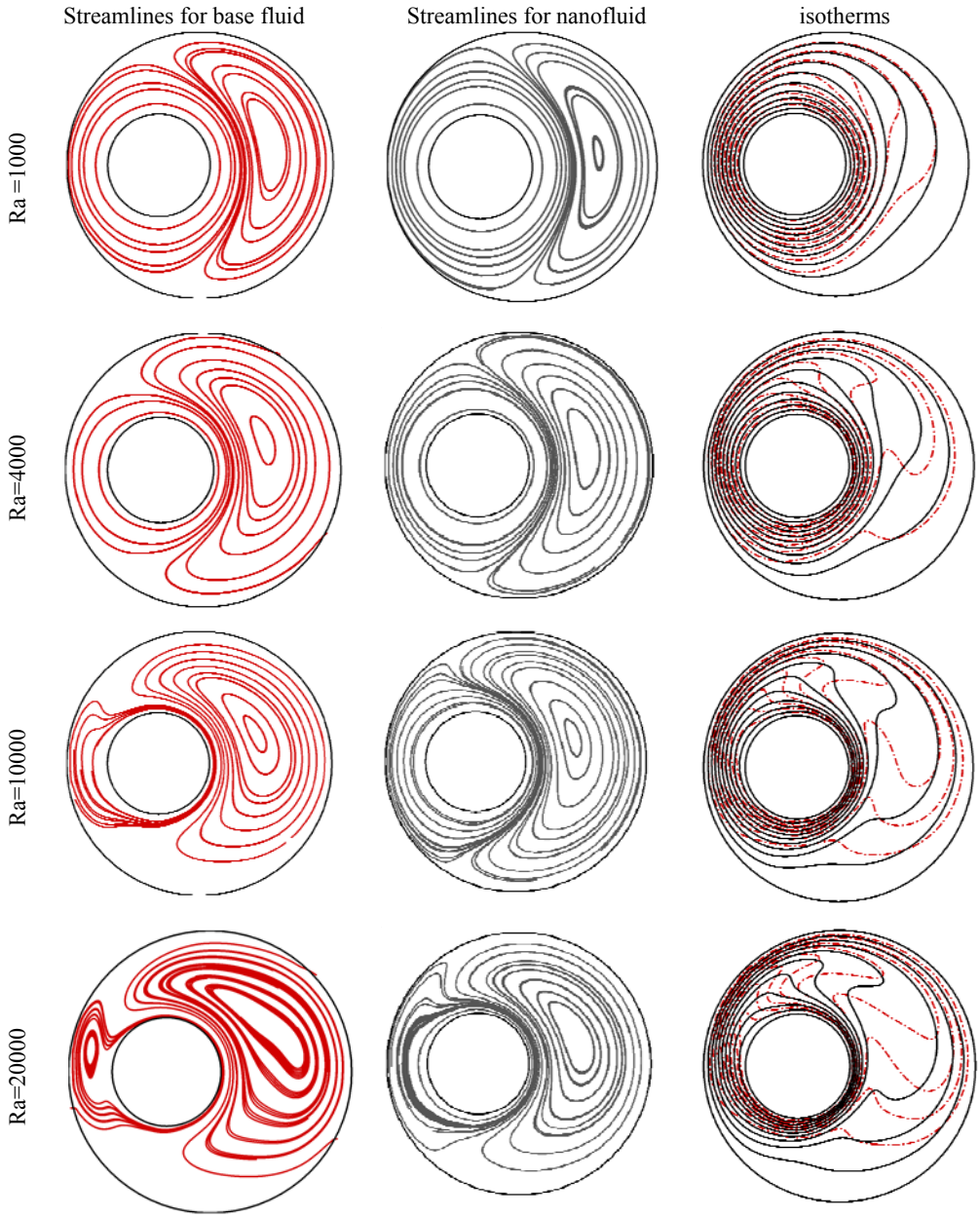

Fig. 8. Streamlines and isotherms patterns for nanofluid (solid line) and base fluid (dash line) at various Rayleigh number, Re=25, e= (1/2, π/2).

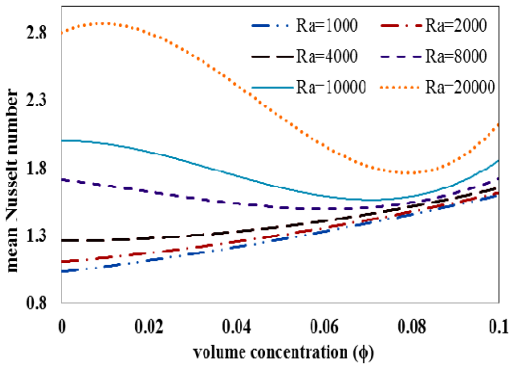

Fig. 9. Effect of volume fraction and Rayleigh number on mean Nusselt number at Re=25, e= (-1/2, π/2).

the bottom of annulus. At the bottom of annulus, the temperature gradient is low, hence it seems that the driving force (buoyancy) is not large enough to disperse and move the nanoparticles.

The local Nusselt number distribution on the inner and outer cylinders for the base fluid and nanofluid with $\phi = 0.05$, at Ra=10^3 and $Ra = 2\times10^4$ is illustrated in Fig. 14. As pointed out earlier, heat transfer of mixed convection in eccentric annuli is influenced by various factors such as eccentricity, buoyant and centrifugal forces thus the local heat flux is non-uniform. Moreover, when the nanoparticles are added to the base fluid, the nanoparticles distribution might become non-uniform and affect the local heat transfer. The

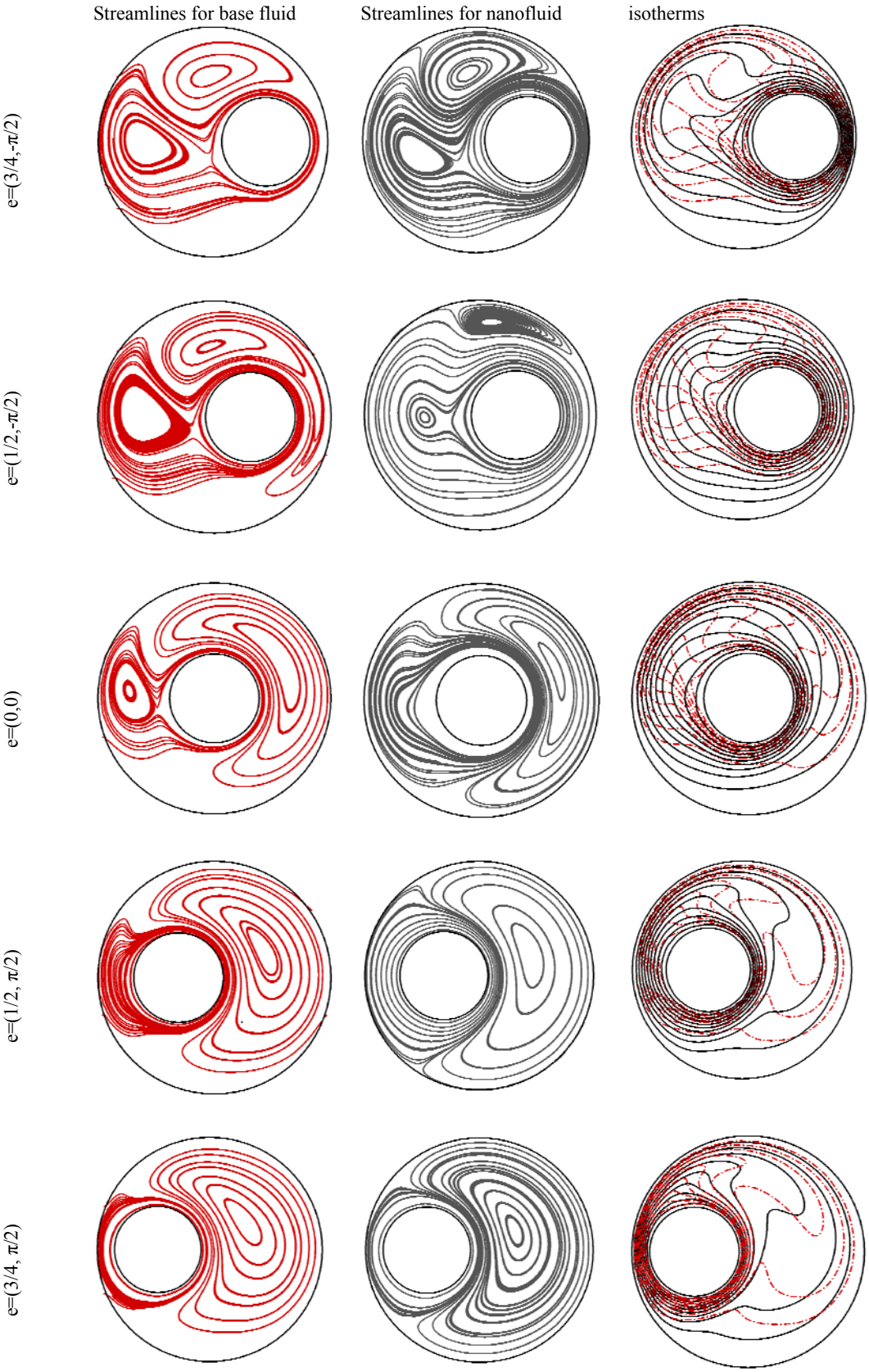

Fig. 10. Streamlines and isotherms patterns for base fluid and nanofluid under different horizontal eccentricity location at Ra=10^4, Re=25.

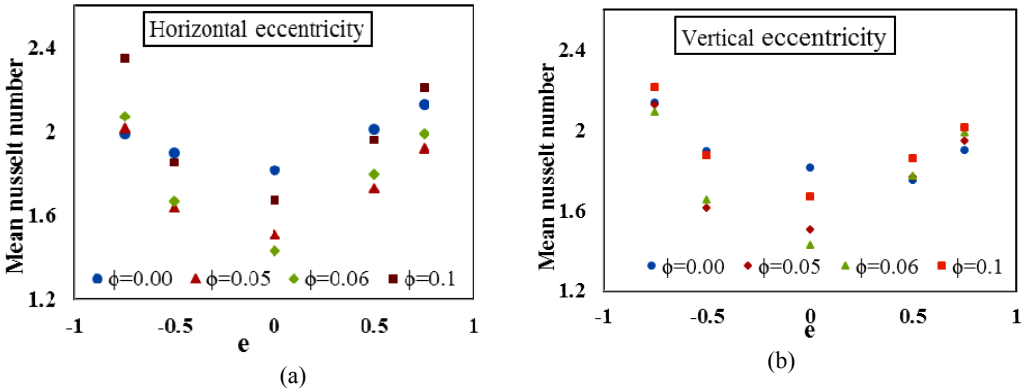

Fig. 11. Effect of eccentricity and volume faction of nanoparticles on mean Nusselt number at Ra=10^4 and Re=25.

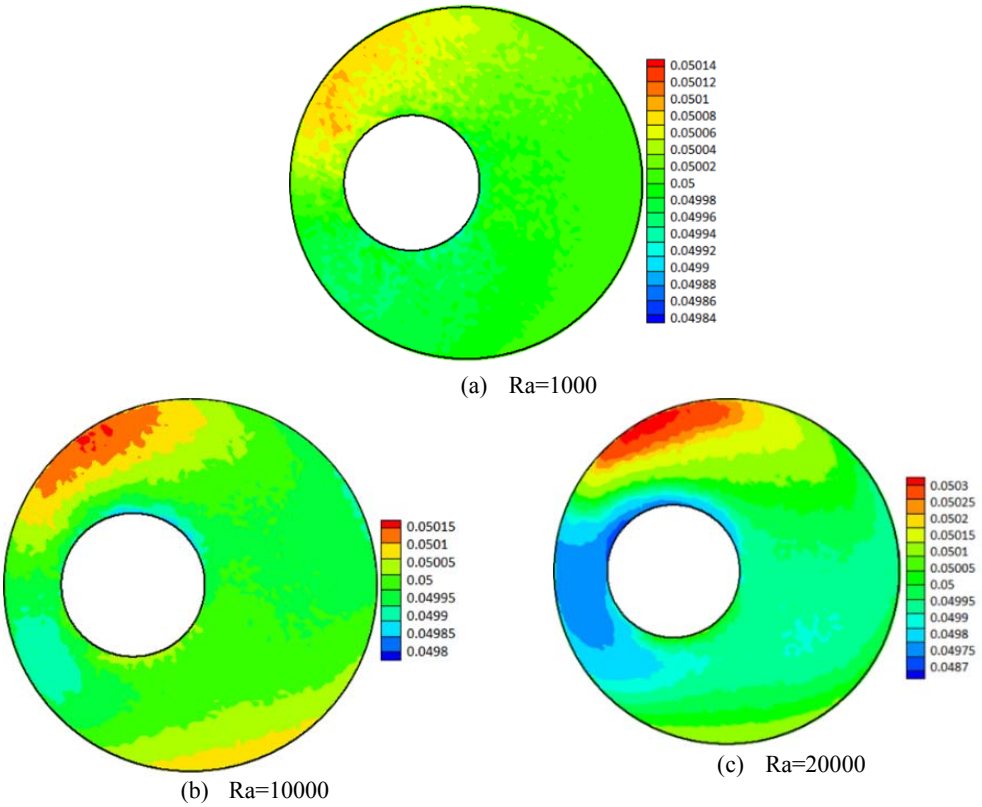

Fig. 12. Nanoparticle volume fraction for different Rayleigh number for □=0.05 and Re=25: (a) Ra=1000, (b) Ra=10000, (c) Ra=20000.

nanoparticles distribution in Ra=10^3 is approximately uniform as it is shown in Fig. 12. The variations in Nusselt number for the base fluid and nanofluid have the same trend (Fig. 14) and the local Nusselt number for nanofluid is larger than the base fluid due the fact that the conduction heat transfer in low Rayleigh number is a dominant mechanism in the heat transfer.

Under the high temperature gradient, at $Ra = 2\times10^4$, the maximum local Nusselt number on the outer cylinders approximately occurs at $\theta = 40^\circ$. The mentioned value for the nanofluid is smaller than that of the base fluid, because the temperature gradient is reduced as the nanoparticles are mostly concentrated in the angular position $0 < \theta < 50^\circ$, shown in Fig. 12. Although, the mean Nusselt number of the nanofluid is smaller than the base fluid, in the regions where conduction heat transfer is dominant $\left(120^\circ < \theta < 270^\circ\right)$, the local Nusselt number increases by the addition of nanoparticles. Besides, on the inner cylinder, the minimum of local heat flux takes place at $\theta = 60^\circ$. It is enhanced due to the existence of nanoparticles. Also, addition of the nanoparticles reduces the difference between the maximum and the minimum Nusselt number. It should be noted that the

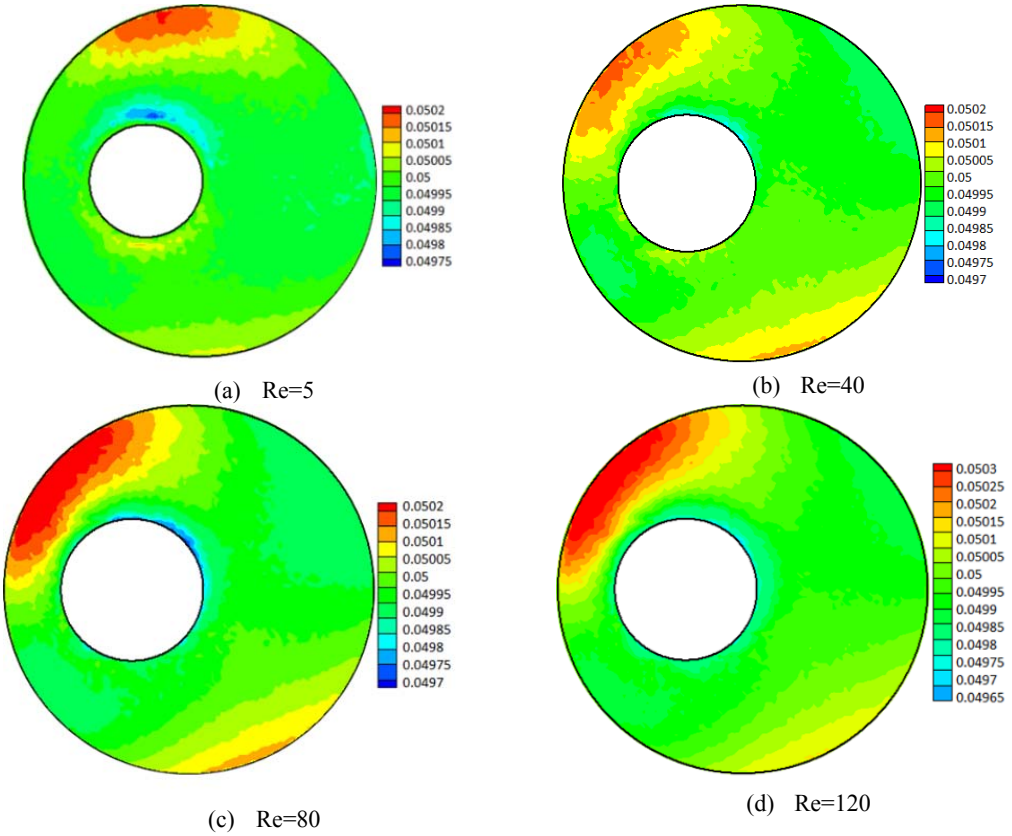

(a) Re=5 (b) Re=40

(c) Re=80 (d) Re=120

Fig. 13. Nanoparticle volume fraction at Ra=10^4 and □=0.05: (a) Re=5, (b) Re=40, (c) Re=80, (d) Re=120.

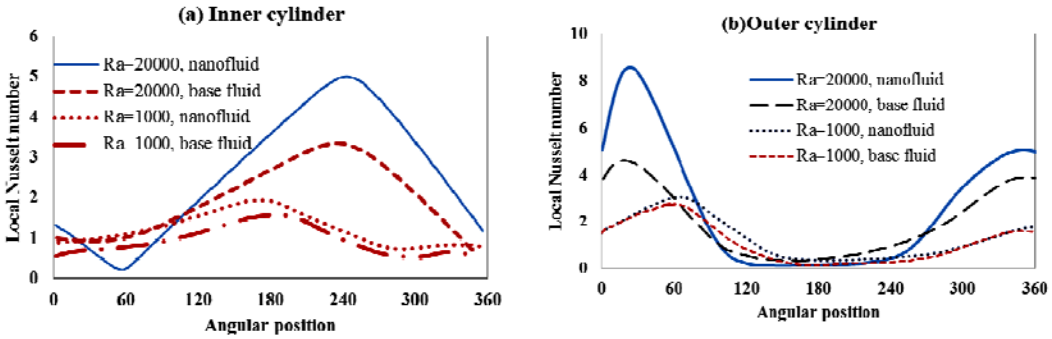

Fig. 14. Local Nusselt number variation at the inner (a) and the outer (b) cylinders for $\varphi = 0$ *and* $\varphi = 0.05$ at $Ra = 10^3$ *and* $Ra = 2\times10^4$.

deviation from the uniform nanoparticles distribution at $Ra = 2\times10^4$ is almost $\pm 3\%$ so the effect of nanoparticles agglomeration on the heat transfer flux is negligible.

5. CONCLUSION

In the present article, the mixed convection heat transfer of a nanofluid in a horizontal annulus with a rotating inner cylinder is simulated with Lattice Boltzmann method. In doing so, the role of nanoparticles in the flow and heat transfer characteristic are considered. The main results are summarized as follows:

1- For fixed Ra and e (eccentricity), when Reynolds number is high, increasing nanoparticles concentration leads to an increase in Nusselt number.

2- For fixed Re and e, when Rayleigh number is low, increasing nanoparticles concentration results in an increase in Nusselt number.

3- For fixed Ra and Re, when the inner cylinder is located above the center, by increasing nanoparticles concentration, the Nusselt number increases.

The above results are extracted from the configurations of streamlines and isotherms of the tested cases. In general, by adding the nanoparticles, the strength of vortices reduces and the thermal plume becomes more uniform compared with the base fluid. When convection is the dominant mode of heat transfer (e.g. the case of high Reynolds number), by increasing the nanoparticle volume fraction the Nusselt number decreases. On the other hand, when conduction plays an effective role in the heat transfer (such as low Rayleigh number), this phenomenon is reversed. In addition, under the assumptions of the current study, increasing Reynolds and Rayleigh numbers leads to an increase in non-uniformity of nanoparticles distribution. Finally, the present results reveal that the multicomponent Lattice Boltzmann method is a powerful tool for simulation of mixed convection heat transfer of nanofluids with curved boundary conditions.

REFERENCES

Abedini, A., A. B. Rahimi and A. Kianifar (2014). Numerical study of mixed convection in the annulus between eccentric rotating cylinders. *Scientia Iranica* 21(14), 1403-1414.

Abu-Nada, E. (2009). Effects of variable viscosity and thermal conductivity of Al 2 O 3–water nanofluid on heat transfer enhancement in natural convection. *International Journal of Heat and Fluid Flow* 30(4), 679-690.

Abu-Sitta, N. H., K. Khanafer, K. Vafai and A. M. Al-Amiri (2007). Combined forced-and natural-convection heat transfer in horizontally counterrotating eccentric and concentric cylinders, *Numerical Heat Transfer, Part A: Applications* 51(12), 1167-1186.

Ashorynejad, H. R., A. A. Mohamad and M. Sheikholeslami (2013). Magnetic field effects on natural convection flow of a nanofluid in a horizontal cylindrical annulus using Lattice Boltzmann method. *International Journal of Thermal Sciences* 64, 240-250.

Bejan, A. (2013). *Convection heat transfer*. John wiley and sons.

Buick, J. and C. Greated (2000). Gravity in a lattice Boltzmann model. *Physical Review E* 61(5), 5307.

Char, M. I. and Y. H. Hsu (1998). Computation of buoyancy-driven flow in an eccentric centrifugal annulus with a non-orthogonal collocated finite volume algorithm. *International journal for numerical methods in fluids* 26(3), 323-343.

Chol, S. (1995). Enhancing thermal conductivity of fluids with nanoparticles. *ASME-Publications-Fed* 231, 99-106.

Cianfrini, M., M. Corcione and A. Quintino (2011). Natural convection heat transfer of nanofluids in annular spaces between horizontal concentric cylinders. *Applied thermal engineering* 31(17), 4055-4063.

Fan, J. and L. Wang (2011). Review of heat conduction in nanofluids. *Journal of Heat Transfer* 133(4), 040801.

Fattahi, E., Farhadi, M. and Sedighi, K. (2011). Lattice Boltzmann simulation of mixed convection heat transfer in eccentric annulus. *International Communications in Heat and Mass Transfer* 38(8), 1135-1141.

Guj, G. and F. Stella (1995). Natural convection in horizontal eccentric annuli: numerical study. *Numerical Heat Transfer, Part A: Applications* 27(1), 89-105.

He, C. and G. Ahmadi (1999). Particle deposition in a nearly developed turbulent duct flow with electrophoresis. *Journal of Aerosol Science* 30(6), 739-758.

He, X. and L. S. Luo (1997). Theory of the lattice Boltzmann method: From the Boltzmann equation to the lattice Boltzmann equation. *Physical Review E* 56(6), 6811.

Huang, H., T. Lee and C. Shu (2006). Thermal curved boundary treatment for the thermal lattice Boltzmann equation. *International Journal of Modern Physics C*, 17(05), 631-643.

Inamuro, T., M. Yoshino and F. Ogino (1995). A non-slip boundary condition for lattice Boltzmann simulations. *Physics of Fluids (1994-present)* 7(12), 2928-2930.

Matin, M. H. and I. Pop (2013). Natural convection flow and heat transfer in an eccentric annulus filled by Copper nanofluid. *International Journal of Heat and Mass Transfer* 61, 353-364.

Mohamad, A. A. (2011). *Lattice Boltzmann method: fundamentals and engineering applications with computer codes*. Springer Science and Business Media.

Parvin, S., R. Nasrin, M. Alim, N. Hossain and A. J. Chamkha (2012). Thermal conductivity variation on natural convection flow of water–alumina nanofluid in an annulus. *International Journal of Heat and Mass Transfer* 55(19), 5268-5274.

Prud'homme, M., L. Robillard and M. Hilal (1993). Natural convection in an annular fluid layer rotating at weak angular velocity, *International journal of heat and mass transfer* 36(6), 1529-1539.

Russel, W. B., D. A. Saville and W. R. Schowalter (1992). *Colloidal dispersions*, Cambridge University press.

Saidur, R., S. Kazi, M. Hossain, M. Rahman and H. Mohammed (2011). A review on the performance of nanoparticles suspended with refrigerants and lubricating oils in refrigeration systems. *Renewable and Sustainable Energy Reviews* 15(1), 310-323.

Sarkar, J. (2011). A critical review on convective heat transfer correlations of nanofluids. *Renewable and Sustainable Energy Reviews* 15(6), 3271-3277.

Shahi, M., A. H. Mahmoudi and F. Talebi (2011). A numerical investigation of conjugated-natural convection heat transfer enhancement of a nanofluid in an annular tube driven by inner heat generating solid cylinder. *International Communications in Heat and Mass Transfer* 38(4), 533-542.

Trisaksri, V. and S. Wongwises (2007). Critical review of heat transfer characteristics of nanofluids. *Renewable and Sustainable Energy Reviews* 11(3), 512-523.

Wang, X. Q. and A. S. Mujumdar (2007). Heat transfer characteristics of nanofluids: a review. *International journal of thermal sciences* 46(1), 1-19.

Wen, D., G. Lin, S. Vafaei and K. Zhang (2009). Review of nanofluids for heat transfer applications. *Particuology 7(2), 141-150.*

Xuan, Y. and Z. Yao (2005). Lattice Boltzmann model for nanofluids. *Heat and mass transfer* 41(3), 199-205.

Yan, Y. and Y. Zu (2008). Numerical simulation of heat transfer and fluid flow past a rotating isothermal cylinder–a LBM approach. *International Journal of Heat and Mass Transfer* 51(9), 2519-2536.

Yu, Z. T., X. Xu, Y. C. Hu, L. W. Fan and K. F. Cen (2012). A numerical investigation of transient natural convection heat transfer of aqueous nanofluids in a horizontal concentric annulus. *International Journal of Heat and Mass Transfer* 55(4), 1141-1148.

Zarghami, A., S. Ubertini and S. Succi (2013). Finite-volume lattice Boltzmann modeling of thermal transport in nanofluids. *Computers and Fluids* 77, 56-65.

Zhou, L., Y. Xuan and Q. Li (2010). Multiscale simulation of flow and heat transfer of nanofluid with lattice Boltzmann method. *International Journal of Multiphase Flow* 36(5), 364-374

.